OXFORD

Human Molecular Genetics, 2021, Vol. 30, No. 1 5–20

doi: 10.1093/hmg/ddaa281
Advance Access Publication Date: 4 January 2021
General Article

GENERAL ARTICLE

Loss of FEZ1, a gene deleted in Jacobsen syndrome, causes locomotion defects and early mortality by impairing motor neuron development

Saravanan Gunaseelan[1,§,†], Ziyin Wang[2,§], Venetia Kok Jing Tong[1,2], Sylvester Wong Shu Ming[1], Rafhanah Banu Bte Abdul Razar[1], Sumitra Srimasorn[1], Wei-Yi Ong[3], Kah-Leong Lim[2,4,§] and John Jia En Chua[1,5,6,7,8,*,§,‡]

[1]Department of Physiology, Yong Loo Lin School of Medicine, National University of Singapore, Singapore, Singapore, [2]National Neuroscience Institute, Singapore, Singapore, [3]Department of Anatomy, Yong Loo Lin School of Medicine, National University of Singapore, Singapore, Singapore, [4]Lee Kong Chian School of Medicine, Nanyang Technological University, Singapore, Singapore, [5]LSI Neurobiology Programme, National University of Singapore, Singapore, Singapore, [6]Healthy Longevity Translational Research Program, Yong Loo Lin School of Medicine, National University of Singapore, Singapore, Singapore, [7]Institute for Health Innovation and Technology, National University of Singapore, Singapore, Singapore and [8]Institute of Molecular and Cell Biology, Agency for Science, Technology and Research (A*STAR), Singapore, Singapore

*To whom correspondence should be addressed at: Department of Physiology, National University of Singapore, 2 Medical Drive MD9, Singapore 117593, Singapore. Tel: +65 6601 5178; Fax: +65 6777 3271; Email: phsjcje@nus.edu.sg

Abstract

FEZ1-mediated axonal transport plays important roles in central nervous system development but its involvement in the peripheral nervous system is not well-characterized. *FEZ1* is deleted in Jacobsen syndrome (JS), an 11q terminal deletion developmental disorder. JS patients display impaired psychomotor skills, including gross and fine motor delay, suggesting that *FEZ1* deletion may be responsible for these phenotypes, given its association with the development of motor-related circuits. Supporting this hypothesis, our data show that FEZ1 is selectively expressed in the rat brain and spinal cord. Its levels progressively increase over the developmental course of human motor neurons (MN) derived from embryonic stem cells. Deletion of *FEZ1* strongly impaired axon and dendrite development, and significantly delayed the transport of synaptic proteins into developing neurites. Concurring with these observations, *Drosophila unc-76* mutants showed severe locomotion impairments, accompanied by a strong reduction of synaptic boutons at neuromuscular junctions. These abnormalities were ameliorated by pharmacological activation of UNC-51/ATG1, a FEZ1-activating kinase, with rapamycin and metformin. Collectively, the results highlight a role for FEZ1 in MN development and implicate its deletion as an underlying cause of motor impairments in JS patients.

[†]Saravanan Gunaseelan, http://orcid.org/0000-0002-4593-8743
[‡]John Jia En Chua, http://orcid.org/0000-0002-5615-1014
[§]Contributed equally to this work.

Received: August 26, 2020. **Revised:** December 10, 2020. **Accepted:** December 23, 2020

Introduction

The elaboration of neuronal processes and synaptic specializations during early neuronal development is a logistically intensive process dependent on the synthesis and movement of large quantities and varieties of biomolecules (1). Anterograde movement of biomolecules in neurons with their highly branched and elongated dendritic and axonal projections presents tremendous challenges (2,3). Not surprisingly, perturbations in neuronal transport, along with mutations in genes encoding transport proteins, have been uncovered in an increasing number of neurological disorders (4,5).

Delivery of newly synthesized components to sites of growth and differentiation relies heavily on microtubule-based Kinesin motor complexes, with motor adapters playing critical roles in cargo binding and modulation of transport through recruitment of regulatory signaling pathways (3,6). A number of adapters have been identified for Kinesin-1 (also known as conventional kinesin or KIF5), including syntabulin and Milton, both of which participate in Kinesin-1's movement of mitochondria along neuronal axons (7–9). We and others identified FEZ1/UNC-76 as a Kinesin-1 adapter in the delivery of synaptic proteins (10–12). Perturbation of UNC-76 function led to formation of axonal cargo aggregates in mutant *Drosophila* and *Caenorhabditis elegans* (11–13). Likewise, perturbation of the kinases ATG1/UNC-51 or PAR-1/MARK, both of which regulate FEZ1 function by phosphorylation at the evolutionarily conserved S58/S143 site, also caused axonal transport defects in these organisms (10,11).

While the aforementioned studies have shown the importance of FEZ1/UNC-76 in transporting synaptic proteins and synapse formation, its role in the development of neurons, in particular of motor neurons (MN), is less well-characterized. Interestingly, locomotion defects were reported for both *Drosophila* and *C. elegans unc-76* mutants (12,14). *Drosophila* harboring germline mutations leading to the loss of UNC-76 expression exhibited progressive paralysis during development and eventual lethality at late larval stages (12). However, whether these phenotypes arose from defects in neural circuits coordinating locomotion or originated from a MN-specific dysfunction is unclear. Likewise, the underlying mechanisms and functional consequences arising from the loss of the protein in specific neuronal populations were not clarified.

Significantly, the *FEZ1* gene is frequently deleted in patients diagnosed with Jacobsen syndrome (JS), a rare and poorly understood chromosomal disorder where the distal region of chromosome 11q is deleted (15–17). JS patients exhibit a number of clinical features including thrombocytopenia, congenital heart disorders and intellectual disability. A substantial proportion of patients also exhibit psychomotor impairment, including gross and fine motor delays, but the gene(s) and underlying mechanisms contributing to this remain poorly defined (17,18).

Here, we demonstrate for the first time the involvement of FEZ1 in human MN development. We show that FEZ1 expression is switched on following differentiation of neuroprogenitors into MNs and that abolishment of its expression in these neurons strongly impairs their development. To further determine whether these abnormalities ultimately affect organismal movement, we examined locomotion using *Drosophila*, a well-established model used to study locomotive behavior. Strikingly, germline deletion as well as MN-specific reduction of UNC-76 expression in *Drosophila* disrupted movement at the larval (crawling) and adult (climbing) stages. The numbers of synaptic boutons at neuromuscular junctions were significantly reduced in mutant larvae. Moreover, we showed that pharmacological enhancement of FEZ1 function via UNC-51 activation rescues the synaptic and locomotion defects associated with its deficiency. Taken together, these results unmask a critical role for FEZ1 in MN development and locomotive behavior, thereby highlighting how loss of FEZ1 can contribute to motor impairment in JS patients.

Results

FEZ1 is primarily expressed in the brain and spinal cord

Previous studies in *C. elegans* reported locomotion defects in *unc-76 mutants* (14). Expression of human FEZ1 in these mutants was able to partially rescue these defects. Thus, like its nematode ortholog, mammalian FEZ1 is likely to be necessary for movement in higher organisms. To begin elucidating this and to assess if FEZ1 could contribute to motor defects present in JS patients, we first re-examined its tissue expression pattern in mammals. Previous studies have mostly employed northern blotting and *in situ* hybridization methods to survey FEZ1 tissue expression at the mRNA level in mice (19,20). To examine FEZ1 expression at the protein level, we probed lysates from adult (3-week) rat tissues obtained from various brain regions, spinal cord and peripheral tissues (heart and lung) using a FEZ1-specific antibody we generated previously (13). In agreement with previous studies using *in situ* RNA hybridization, FEZ1 is highly expressed in the brain where it shows region specificity, with highest levels detected in the temporal lobe, pre-frontal cortex and cerebellum (Fig. 1A and B). Notably, FEZ1 was not detected in peripheral tissues such as the heart or lung, supporting that its expression is restricted to nervous tissues. Importantly, significant levels of FEZ1 were present in the spinal cord, a tissue that is required for movement (21).

Immunohistological staining of tissue sections corroborated the immunoblot analyses, showing expression of FEZ1 in the brain as well as the spinal cord and further highlighted its expression in neuronal cells. In the cerebral neocortex, both pyramidal and non-pyramidal neurons were immunolabeled for FEZ1 with the exception of spiny stellate cells in layer IV (Fig. 1Ca). Likewise, the hippocampus also showed strong expression of FEZ1, with labeling observed in pyramidal cell bodies and their apical dendrites in the CA fields (Fig. 1Cb), and in dentate granule (DG) neurons and mossy fibers (MF) in the stratum lucidum of CA3 (Fig. 1Cc). Dense labeling of putative, cholinergic neurons was also observed in the medial septum (MS, Fig. 1Cd). The striatum, including the caudate-putamen (CPU) was moderately labeled, in contrast to the globus pallidus (GP) which was very lightly labeled or unlabeled (Fig. 1Ce). The cerebellar molecular layer (ML) and Purkinje cell layer were also densely labeled but FEZ1 expression in the granule cell layer was not observed (Fig. 1Cf). In the spinal cord, the superficial laminae of the dorsal horn (DH) were very densely labeled (Fig. 1Cg) while dense labeling was also observed in MNs in the ventral horn (VH, Fig. 1Ch). Collectively, these results indicate that, like in CNS neurons, FEZ1 expressed in peripheral MNs could play essential roles in their development and function.

Expression of FEZ1 accompanies differentiation and maturation of human motor neurons

While FEZ1 function in mammalian CNS neurons has been studied, its role in the mammalian peripheral nervous system remains unknown. Previous studies in *C. elegans* have implicated a role of UNC-76 in the development and projection of MN

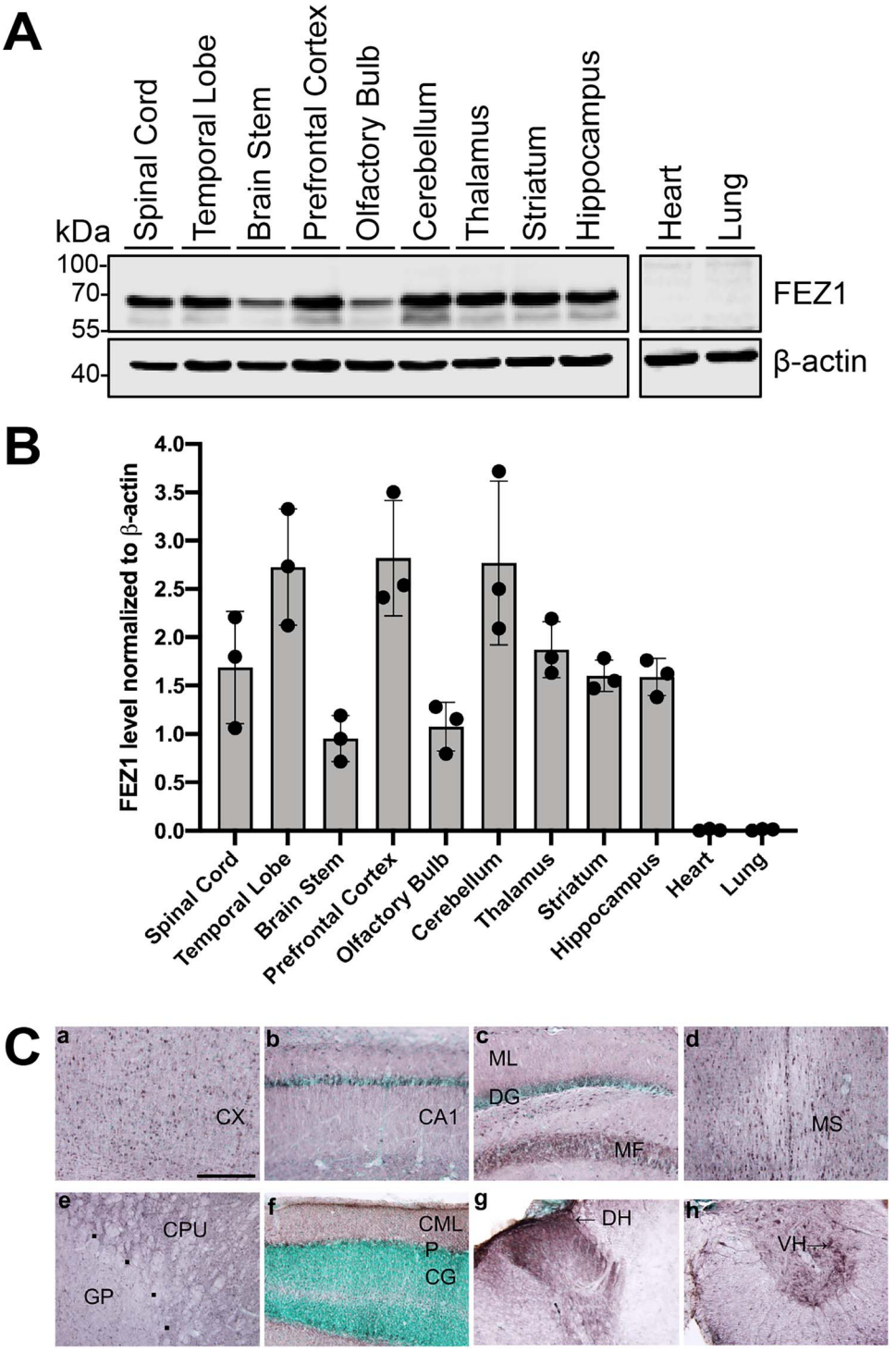

Figure 1. FEZ1 is differentially expressed in various brain regions and spinal cord but absent in peripheral tissues. (**A**) Immunoblot analyses of FEZ1 in rat spinal cord and various parts of the rat brain (temporal lobe, brain stem, prefrontal cortex, olfactory bulb, cerebellum, thalamus, striatum and hippocampus) and peripheral tissues (heart and lung). β-actin was used as a loading control. (**B**) Quantification of FEZ1 protein normalized against β-actin. FEZ1 protein levels were high in most brain regions tested with the exception of the brain stem and olfactory bulb where comparatively lower amounts of FEZ1 were present. Peripheral tissues such as the heart and lung did not express FEZ1. (**C**) Sections of the rat brain and spinal cord were stained by immunoperoxidase for FEZ1 and counterstained with methyl green. (**a**) Layers V and VI of the frontal cortex (CX), showing many labeled neurons. (**b**) Field CA1 of the hippocampus, showing labeled pyramidal neurons. (**c**) Dentate gyrus, showing dense labeling of DG cell bodies, their dendrites in the ML, and their axons or MF in the stratum lucidum of CA3. (**d**) MS showing many densely labeled neurons. (**e**) CPU showing moderately labeled neurons. In contrast, the GP is very lightly labeled or unlabeled. (**f**) Cerebellar cortex showing dense labeling of Purkinje neuronal cell bodies (P) and their dendrites in the ML (CML). In contrast, the cerebellar granule (CG) neurons are unlabeled; these are counterstained by methyl green. (**g**) DH of the spinal cord, showing dense labeling of the superficial laminae. (**h**) VH of the spinal cord, showing dense staining of MNs. Scale bar represents 200 µm. Data are expressed as the average with error bars representing ±SD from three independent experiments ($n = 3$).

axons (14,22). However, whether its mammalian ortholog could also play similar roles in human MN development has not been established.

To determine this, we generated cholinergic human MNs derived from human embryonic stem cells (hESCs) using a previously published protocol (23). The hESCs were sequentially differentiated into neuroepithelial progenitor cells (NEP) and OLIG2$^+$ MN progenitor (MNP) cells (Supplementary Material, Fig. S1A and B). At each stage, cells were validated by staining against their appropriate stage-specific markers (hESCs: Nanog$^+$, Lin28a$^+$, SOX2$^+$; NEP: Nestin$^+$, SOX2$^+$; OLIG2$^+$: OLIG2$^+$, SOX2$^+$). The immature neuronal marker (TUJ) and MN markers such as HB9 and ISL1 were absent, indicating that no spontaneous differentiation into neuronal cells had occurred (24) (Supplementary Material, Fig. S1C–F). In the final conversion step, OLIG2$^+$ MNPs were differentiated into MNs. Bright field images showed cellular processes emanating from cell bodies appearing as early as 2 days after differentiation that continued to elongate over the period of investigation (DIV9 to DIV21) (Supplementary Material, Fig. S2A). Neuronal cell bodies progressively migrated towards each other forming clusters and eventually spheres, as seen in DIV14 and 21.

To confirm that the differentiating cells were indeed cholinergic MNs, immunofluorescence staining was performed using MN specific markers at DIV9, 14 and 21 (Fig. 2A). Expression of the choline acetyltransferase (ChAT) was detectable as early as DIV9 and its levels progressively increase with development (Fig. 2A; Supplementary Material, Fig. S2B). Likewise, strong TUJ and neurofilament H (detected using the SMI32 antibody) signals were present in the developing MNs at all time points observed (Fig. 2A). In addition, the neurons also stained positive for ISL1 (Supplementary Material, Fig. S2C). We did not observe differences in MNs derived from distinct passages of OLIG2$^+$ neuroprogenitor cells (P0 to P2). Collectively, these results confirmed the successful generation of human MNs from hESCs.

To examine FEZ1 expression during MN differentiation and development, cell lysates collected from hESC, NEP, OLIG2$^+$ MNP and MNs at various time points were analyzed by immunoblotting. OLIG2 was only detectable in OLIG2$^+$ MNPs, whereas the neuronal markers Synapsin 1, neurofilaments heavy (NF-H), medium (NF-M) and light (NF-L) chains, and ISL1 were only observed in developing MNs but not in hESCs, NEPs and MNPs (Fig. 2B). FEZ1 became detectable in MNs 9 days after differentiation from OLIG2$^+$ MNP (the earliest time point used in this study) but not at the earlier progenitor stages. Its expression continued to increase as the neurons developed for 14 and 21 days, respectively (Fig. 2B and C). In particular, this increase coincided with the appearance and increase in levels of Synapsin 1, neurofilaments and ISL1 (Fig. 2B).

To examine its distribution within these cells, DIV9 to DIV21 MNs were stained for FEZ1 along with the dendritic and axonal markers MAP2 and Tau, respectively (Fig. 2D; Supplementary Material, Fig. S2D). At DIV9, punctate staining of FEZ1 could be observed along Tau-positive axons extending from neuronal cell bodies (Fig. 2D). While this distribution of FEZ1 was retained at later time points, overlapping of MAP2 and Tau signals at these stages where axons and dendrites begin to bundle made it difficult to distinguish if FEZ1 remains in axons, or as has been observed in hippocampal neurons, also distributed to dendrites (10). Like in hippocampal neurons, FEZ1 could also be seen in growth cones at DIV9 (Fig. 2E). Collectively, these results indicate that FEZ1 expression is switched on when progenitor cells differentiate into MNs and that its levels progressively increase as the neurons mature.

FEZ1 is required for proper axon and dendrite development in human motor neurons

To better understand how FEZ1 contributes to human MN development, we employed CRISPR-Cas9 to abrogate FEZ1 expression in these neurons. MNs at DIV1 were infected with lentiviruses expressing sgRNAs against FEZ1 or a control (LUC). Immunoblotting of the cell lysates at DIV9, DIV14 and DIV21 confirms the successful abrogation of FEZ1 expression in FEZ1 sgRNA-treated but not LUC sgRNA-treated MNs (Fig. 3A and B). Noteworthy, FEZ1-deficient MNs continued to express the neuronal markers Synapsin 1, neurofilaments and ISL1. Likewise, ChAT expression was present in both types of MNs (Supplementary Material, Fig. S3B). These results indicate that while FEZ1 expression is switched on upon MN differentiation, its expression is not required for differentiation neuroprogenitors to MNs.

Strikingly, MAP2$^+$ and Tau$^+$ processes emanating from the cell bodies of FEZ1 sgRNA-treated MNs appeared to be dramatically shortened and underdeveloped as compared with their control counterparts (Fig. 3C; Supplementary Material, Fig. S3A). Quantitative measurements confirmed that both total axon and dendrite lengths were significantly shorter in FEZ1 sgRNA-treated MNs as compared with controls at all three developmental time points examined (Fig. 3D and E). Moreover, by combining Sholl with area under the curve (AUC) analyses, we confirmed that FEZ1 sgRNA-treated MNs exhibited significantly reduced branching as compared with control MNs (Fig. 3F–H) (25). Importantly, FEZ1-deficient neurons do not appear to show signs of degeneration as axons and dendrites remain contiguous throughout the course of maturation and did not appear to exhibit characteristic signs of dystrophy (Fig. 3C) (26).

FEZ1 is an important motor adapter for the transport of proteins involved in neuronal development and synaptic function. Indeed, Piccolo, a key component of active zones in NMJs and a known FEZ1 cargo (10,27), colocalizes with FEZ1 puncta along neurites in MNs (Supplementary Material, Fig. S4). Thus, we wondered if the retardation in neurite development could be attributed to the perturbations in FEZ1-mediated delivery of synaptic components, including Piccolo that is required to support neuronal development. To ascertain this, we immunostained developing MNs for Piccolo at DIV9, DIV14 and DIV21.

Piccolo immunoreactivity was readily observed in axons of control neurons at all three developmental stages. In stark contrast, its appearance in neurites was markedly delayed in FEZ1 sgRNA-treated MNs (Fig. 4A–C). Although Piccolo was already present in proximal and distal neurites at DIV9 of control MNs, it was noticeably absent at this time point in FEZ1 sgRNA-treated MNs, and barely detectable at DIV14 (Fig. 4B and C). This delay in appearance of Piccolo along the neurites in the absence of FEZ1 is consistent with the notion that loss of FEZ1 interferes with the axonal transport of synaptic proteins during neuronal development thereby retarding the development of MNs. Indeed, while the strongest intensity of Piccolo at proximal and distal neurites was observed at DIV9 in control neurons, the highest signal was only observed proximally at DIV21 in FEZ1 sgRNA-treated neurons. Quantification of MNs at all three time points confirmed that a significant population of FEZ1 sgRNA-treated MNs consistently showed reduced or no proximal and distal neurite Piccolo staining as compared with control MNs. Quantitatively, the percentages of FEZ1 sgRNA-treated MNs with Piccolo-positive expression proximally were $5.8 \pm 1.08\%$, $28.9 \pm 1.10\%$ and $50.1 \pm 1.81\%$ at DIV9, DIV14 and DIV21, respectively. In comparison, the percentages of control neurons with

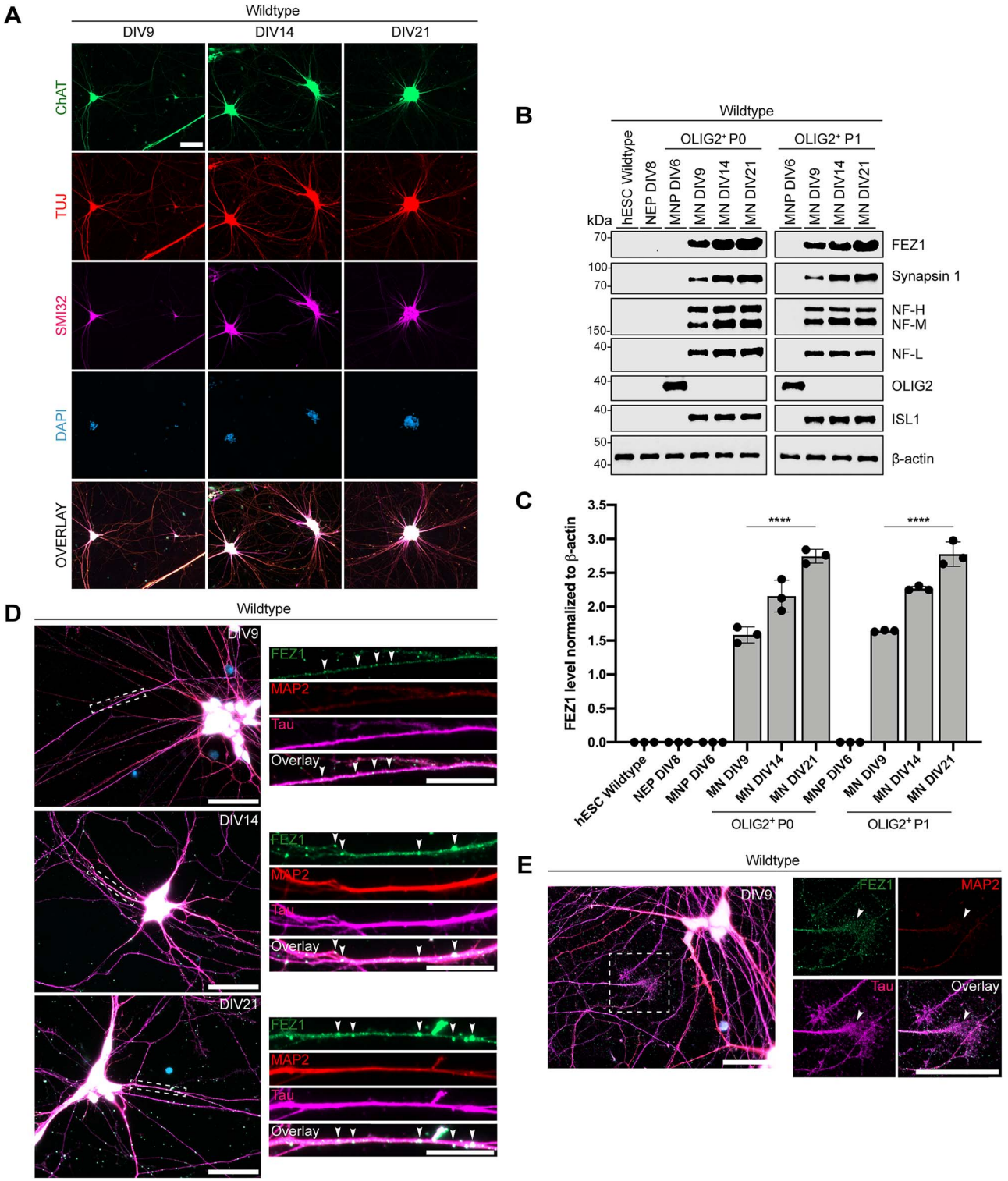

Figure 2. Onset of FEZ1 expression coincides with the differentiation of human neuroprogenitor stem cells into MNs and increases during their maturation. (**A**) Immunostaining of MN at DIV9, DIV14 and DIV21 with antibodies against ChAT, TUJ and SMI32. Scale bars represent 200 µm. (**B**) Immunoblotting of cell lysates from hESC, neuroprogenitor (NEP, MNP) and developing MNs against FEZ1, ISL1, Synapsin 1, OLIG2 and neurofilaments (NF-L, NF-M and NF-H). β-actin was used as a loading control. (**C**) Quantification of FEZ1 protein level normalized against β-actin. FEZ1 levels became detectable and increased in developing MNs from DIV9 to DIV21. Data are expressed as the average with error bars representing ±SD from three independent experiments. Statistical analyses were performed with one-way ANOVA corrected using Bonferroni's post-test ($^{****}P < 0.0001$). (**D**) MNs at DIV9, 14 and 21 show punctate distribution of FEZ1 in axons (Tau) and dendrites (MAP2) (arrowheads) and (**E**) in growth cones (arrows). Scale bars represent 40 µm.

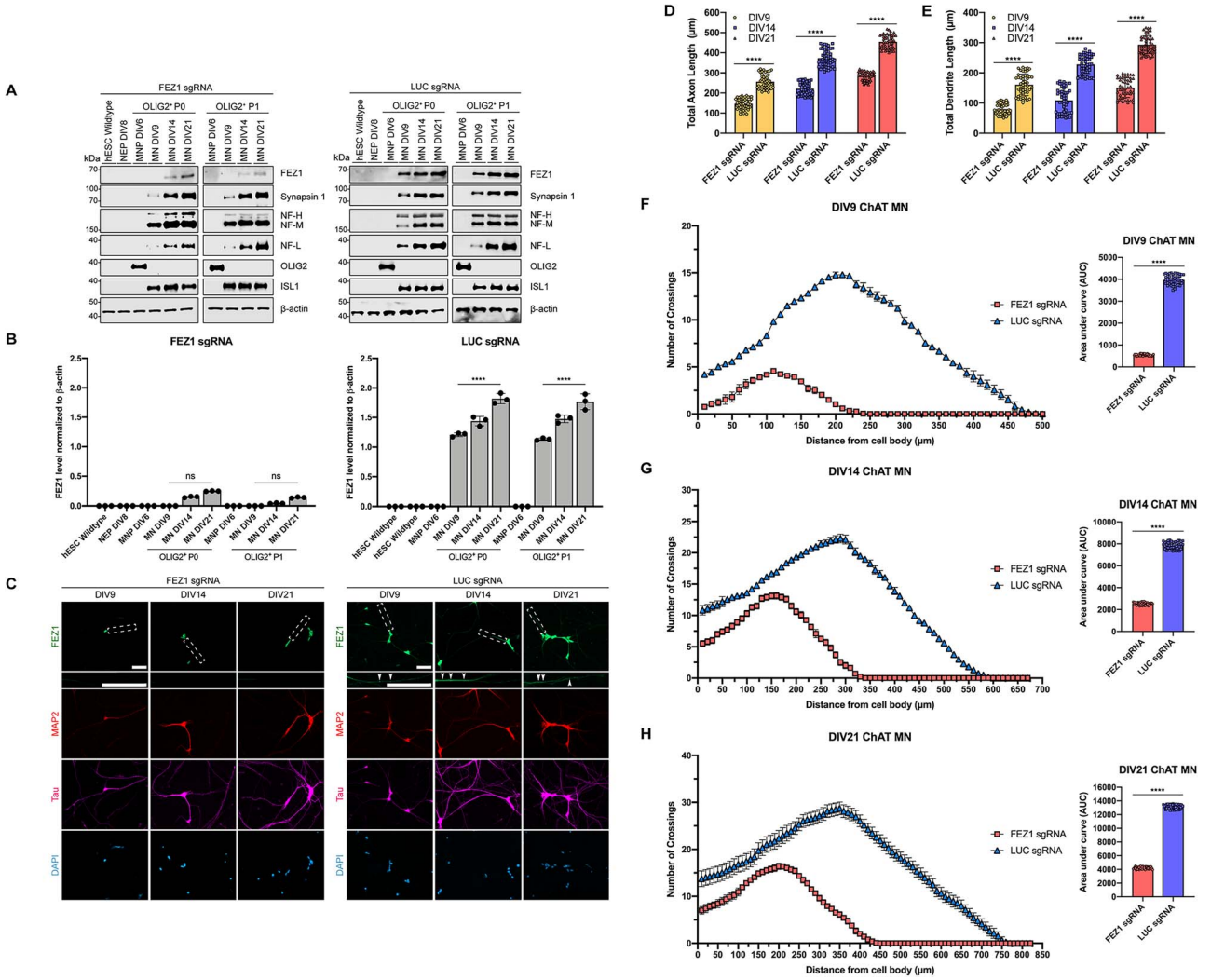

Figure 3. FEZ1-deficient MNs exhibit developmental defects. (**A**) Lysates from developing MNs infected with control (LUC) or FEZ1 sgRNA-expressing lentiviruses were immunoblotted for FEZ1, ISL1, Synapsin 1, OLIG2 and neurofilaments (NF-L, NF-M and NF-H). β-actin was used as a loading control. (**B**) Quantification of FEZ1 protein levels were normalized against β-actin. FEZ1 levels were low in FEZ1 sgRNA-treated MNs as compared with LUC-controls at DIV9, 14 and 21. (**C**) Immunofluorescence assays of MNs with primary antibodies specific to FEZ1, Tau and MAP2. FEZ1 puncta was absent in neurites emanating from FEZ1 sgRNA-treated MNs but present in LUC sgRNA-treated MNs (arrowheads). Scale bars represent 40 μm. (**D** and **E**) Quantification of (D) axons and (E) dendrite lengths in FEZ1 sgRNA-treated MNs ($n = 3$, 66 neurons per set). FEZ1 sgRNA-treated MNs displayed significantly shorter axons and dendrites as compared with control MNs at all DIVs tested. (**F-H**) Sholl analyses of control and FEZ1 sgRNA-treated MNs in (F) DIV9, (G) DIV14 and (H) DIV21 indicate reduced neurite complexity at all DIVs as measured by the respective AUC analyses ($n = 3$, 50 neurons per set). Data are expressed as the average with error bars representing ±SD from three independent experiments. Statistical analyses were performed with one-way ANOVA corrected using Bonferroni's post-test (****$P < 0.0001$).

proximal Piccolo staining were 86.2 ± 1.37%, 89.6 ± 1.42% and 92.5% ± 1.24% at DIV9, DIV14 and DIV21, respectively (Fig. 4D). Consistent with this, reduced percentages of Piccolo-positive distal neurites were observed in FEZ1 sgRNA-treated MNs (DIV9: 1.9 ± 0.55%, DIV14: 15.7 ± 1.38% and DIV21: 27.6 ± 1.50%) in contrast to control neurons (DIV9: 86.4 ± 2.01%, DIV14: 88.5 ± 0.87% and DIV21: 92.2 ± 1.43%) at their corresponding respective timepoints (Fig. 4E).

Of note, no observable difference in Piccolo fluorescence intensity could be discerned in the cell bodies of both types of MNs. This indicated that the delay in axonal appearance of Piccolo is unlikely attributable to alterations in protein synthesis or stability (Fig. 4A). Rather, the defect is most likely due to the loss of FEZ1-mediated transport at the early developmental phase of these neurons. Interestingly, the population of FEZ1 sgRNA-treated MNs bearing proximal Piccolo signal gradually increased over time, indicating that some form of compensatory axonal transport is still retained in these neurons (Fig. 4B and C). In addition to FEZ1, syntabulin also functions as a presynaptic cargo adapter (28). To examine if the latter could partially compensate for the later appearance of the Piccolo in axons of older FEZ1 sgRNA-treated MNs, we also probed for expression of syntabulin in these samples. Intriguingly, syntabulin is only very weakly detected from DIV21 in wildtype, control as well as FEZ1 sgRNA-treated MNs as compared with DIV14 rat hippocampal neurons (RHC) where it is amply expressed (Supplementary Material, Fig. S5A and B) (9). Furthermore, loss of FEZ1 does not trigger a compensatory increase in syntabulin expression in MNs. Thus, syntabulin probably only contributes to cargo transport at later stages of MN development.

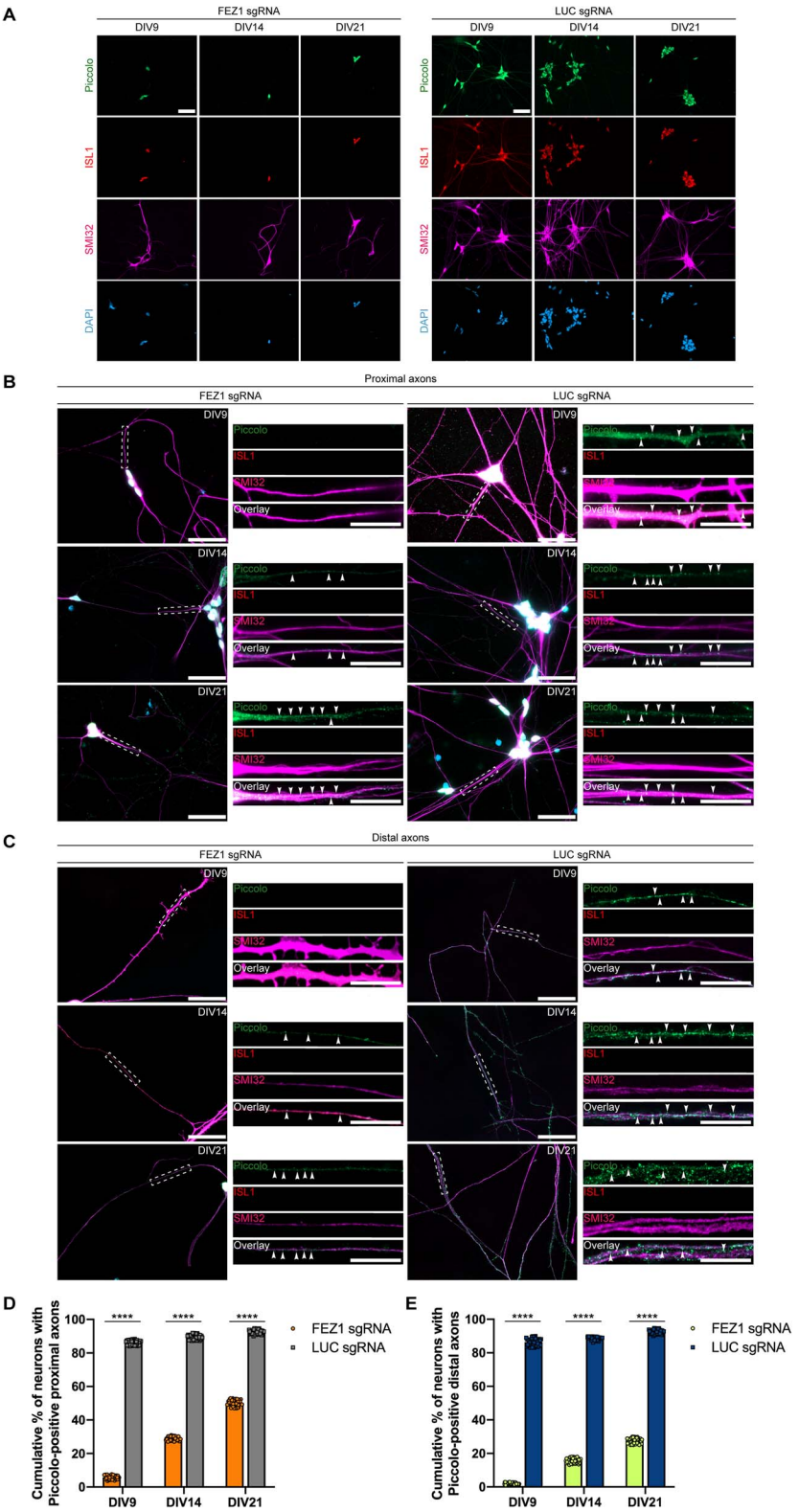

Figure 4. Loss of FEZ1 delays transport of FEZ1 cargoes into developing axons. Control and FEZ1 sgRNA-treated MNs were stained for ISL1, SMI32 and Piccolo at DIV9, 14 and 21. (**A**) Low magnification views of MNs showed strong Piccolo staining in cell bodies of both types of neurons at all time points. Scale bars represent 100 µm. (**B** and **C**) Transport of Piccolo into (B) proximal and (C) distal axons in the form of discrete puncta (arrowheads) was strongly observed starting from DIV9 in control neurons. In contrast, Piccolo signal in axons of FEZ1 sgRNA-treated MNs was undetectable at DIV9 and only faintly detectable starting at DIV14. Scale bars represent 40 µm. (**D** and **E**) Control neurons exhibited Piccolo signal in (D) proximal and (E) distal axons at all stages of development ($n = 3$, 50 neurons per set). Data are expressed as the average with error bars representing ±SD from three independent experiments. Statistical analyses were performed with one-way ANOVA corrected using Bonferroni's post-test (****$P < 0.0001$).

unc-76 deficiency in Drosophila impairs locomotion and increases mortality

Given the requirement of FEZ1 expression in MN development, we were interested to examine the consequences of loss of FEZ1 with regards to movement. In particular, we wanted to assess whether the loss of FEZ1 could contribute to defects in gross and fine motor skills as has been reported in JS patients. We decided to model this behavior using *Drosophila*, an organism that has been extensively used to study locomotion behavior (29,30).

Previously, Gindhart and colleagues alluded to unpublished observations that larvae of *Drosophila unc-76* germline mutants exhibited gradual paralysis over the course of their development (12). However, the origin and extent of the locomotion phenotypes were not detailed. Also, it was unclear if they could have originated from a defect in neural circuits coordinating locomotion or from a MN-specific dysfunction. To examine this further, we generated flies that were heterozygous for *unc-76* mutation and characterized locomotion defects in these flies using crawling and mortality assays. We ascertained the loss of *unc-76* in the mutants via RT-PCR and immunoblotting (Supplementary Material, Fig. S6A–C, G0310/+ lane). Consistent with the previous report, we recorded a significant reduction in crawling performance of the mutants as compared with their wild-type counterparts (Supplementary Material, Fig. S6D) (12). Furthermore, we documented a marked increase in the mortality of adult mutant flies in an age-dependent manner (Supplementary Material, Fig. S6E). Taken together, these results confirmed that loss of UNC-76 in *Drosophila* causes locomotion defects while at the same time increasing mortality.

Next, we assessed if these phenotypic deficits could be recapitulated should UNC-76 be ablated specifically in the MNs. For this purpose, we generated conditional knockdown mutants of *unc-76* specifically in fly MNs using the *D42-GAL4* driver. We first confirmed that *unc-76* expression was indeed downregulated in *Drosophila unc-76* RNAi mutants via the pan-neuronal *Elav*-GAL4 driver as compared with *Elav*/+ controls (Supplementary Material, Fig. S6B and C, *Elav* > *unc76* RNAi lane). A decrease in the levels of expression of the target gene, *unc-76*, was observed in the RNAi mutants, with a reduction of approximately 40% in mRNA levels (Supplementary Material, Fig. S6B). Immunoblots also revealed a corresponding reduction (approximately 30%) in protein levels in the RNAi mutant as compared with the *Elav*/+ control (Supplementary Material, Fig. S6C), confirming that the RNAi approach worked. Encouraged by this, we proceeded to characterize the *D42-GAL4* driven *unc-76* RNAi flies.

As expected, the MN-driven mutants exhibited phenotypes similar to those observed in the germline mutants (Fig. 5A and D; Supplementary Material, Fig. S6D and E). Significant decrease in locomotion (crawling) ability was observed in the *unc-76* RNAi mutant larvae when compared with both the native control (White) and *D42-GAL4*/+ control larvae, where the normalized distance traveled was reduced by approximately 50% in mutant larvae (Fig. 5A). To determine if the locomotion defects could be attributed to MN abnormalities in these mutants, we performed immunohistochemical staining of the larvae NMJ (Fig. 5B). Compared with controls, we observed a visible decrease in synapses, with approximately 40% reduction in the numbers of synaptic boutons in mutant larvae (Fig. 5C). Thus, developmental defects observed early during the development of FEZ1-deficient MNs appear to culminate in synaptic abnormalities that closely correlated with the diminished ability of the organism to move.

Like the germline mutants, *D42* > *unc-76* RNAi flies exhibit markedly increased mortality relative to control flies (Fig. 5D). Interestingly, the motor deficits displayed by *D42* > *unc-76* RNAi mutant larvae persisted into the adult stages but in an age-dependent manner. At day 25 post-eclosion, there were no apparent differences in the climbing abilities between control and mutant flies (Fig. 5E). However, at day 50, we observed dramatically reduced climbing of the mutant flies as compared with their control counterparts (Fig. 5F). Given the pivotal role of UNC-76 in axonal trafficking and synaptic function, we were curious to examine whether deficiency in UNC-76 expression could affect other types of neurons involved in locomotion. Loss of dopaminergic neurons is known to affect climbing in flies (31). To examine if these neurons could also be involved, we generated *Drosophila* lines that express *unc-76* RNAi selectively in dopaminergic neurons via the dopaminergic neuron driver *Ddc*-GAL4. Interestingly, while we recorded a modest decline in the survival of these mutants (Supplementary Material, Fig. S7A), we did not observe any climbing defects in *Ddc*-GAL4 driven *unc-76* RNAi lines up to day 50 post-eclosion (Supplementary Material, Fig. S7B and C). Thus, the loss of UNC-76 function in fly MNs alone appears to be sufficient and critical for recapitulating the overt phenotypic features of the germline mutant. At the same time, these results also support that UNC-76 is important for MN function both at the developmental and post-developmental stages. Importantly, that loss of FEZ1/UNC-76 alone is sufficient to cause locomotion defects reinforces the notion that deletion of the gene can contribute to motor disorders found in JS patients.

Rescue of unc-76 knockdown phenotypes by pharmacological modulators upstream of ATG1/UNC-51

Next, we were keen to examine whether the above pathological phenotypes exhibited by *D42* > *unc-76* RNAi mutant flies could be rescued via a pharmacological approach. *Drosophila* UNC-76 was previously shown to be activated by ATG1/UNC-51 and deletion of the kinase caused synaptic effects similar to those observed in our *unc-76* mutants (11). This suggested that activation of ATG1/UNC-51 could potentially rescue some of the phenotypes in the adapter mutants. We took advantage of the fact that levels of UNC-76 were downregulated but not completely eliminated in the RNAi mutant fly lines (Supplementary Material, Fig. S6C). This renders the possibility to increase the activity of the remaining UNC-76 pool by modulating UNC-51 using several well-characterized drugs that have been shown to selectively enhance the kinase's activity. Accordingly, we treated the flies with several concentrations of 5-amino-1-β-d-ribofuranosyl-imidazole-4-carboxamide (AICAR), metformin and rapamycin that are known to activate ATG1 in order to find an optimized dosing regimen for treatment of our mutant flies (Supplementary Material, Fig. S8) (32–34). Three different concentrations were used for each drug and the climbing assay was used as a readout to determine the optimal dosage for rescue of UNC-76 function (Supplementary Material, Fig. S8B, D and F).

At doses of 1 mM metformin and 200 μM rapamycin, we found that the lifespan of treated flies was significantly improved as compared with DMSO-treated mutants, with an increase in mean lifespan by 14% and 15%, respectively (Fig. 6A; Supplementary Material, Table S1). We found that *Drosophila D42* > *unc-76* RNAi mutant flies treated with these compounds also displayed significantly improved climbing performance over untreated controls at day 50 (Fig. 6B and C). Correlating with this, we observed a marked increase in the number of

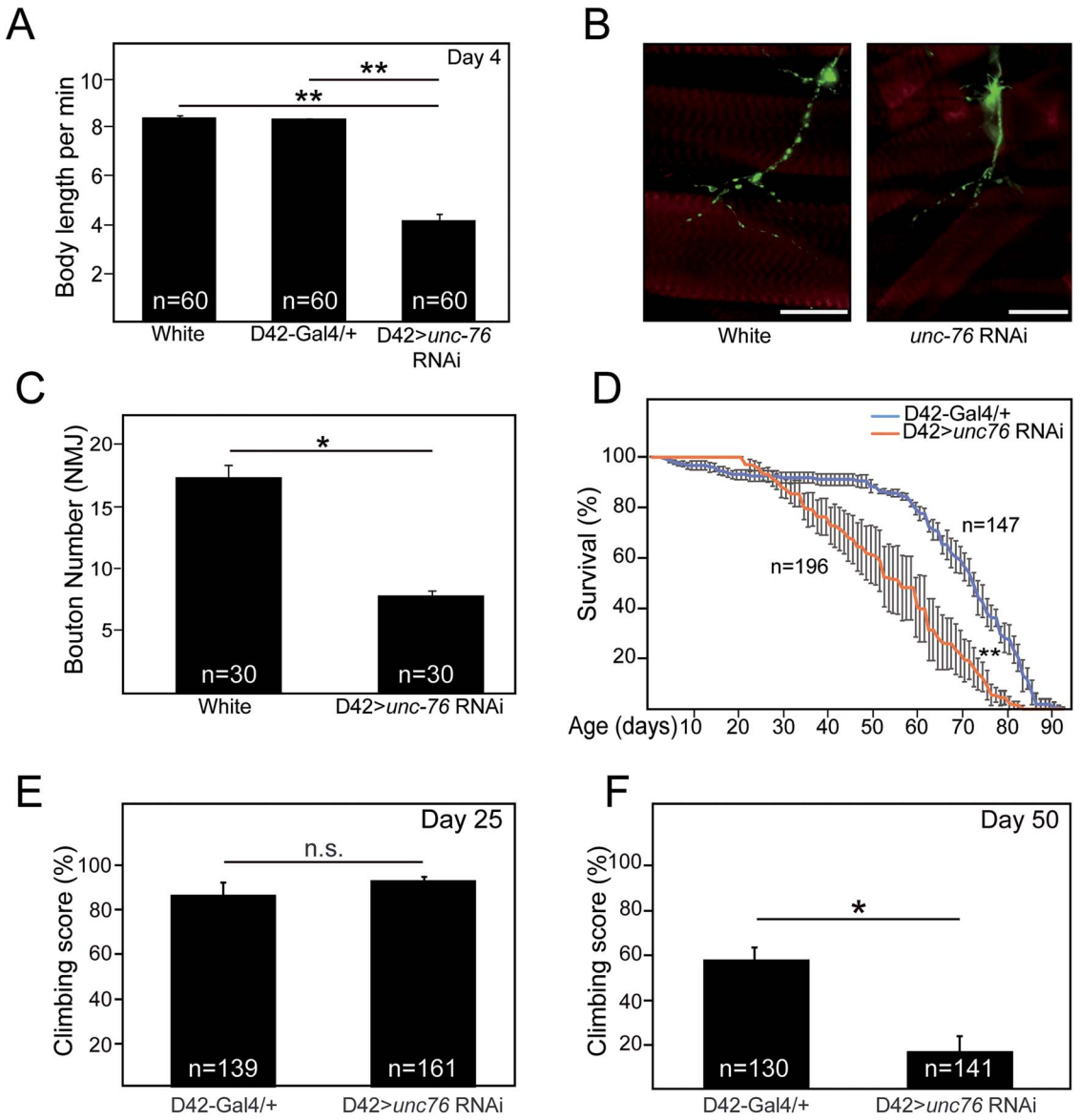

Figure 5. UNC-76-deficient *Drosophila* exhibit defects in locomotion and neuromuscular junctions, accompanied by early lethality. (**A**) Crawling ability of white, *D42*-driven white and *D42*-driven *unc-76* RNAi larvae, as indicated. MN-specific knockdown mutants exhibit locomotion defects ($n = 60$ larvae per genotype). Statistical analyses were performed with one-way ANOVA followed by Bonferroni's *post-hoc* test ($^{**}P < 0.01$). (**B**) Anti-fasciclin and anti-Futsch staining (green) staining for NMJ, and Atto 647 N-Phalloidin (red) staining for muscles as shown for two representative samples: white and *D42*-driven *unc-76* RNAi larvae. Scale bar represents 50 µm. Synaptic boutons were strongly reduced in MNs from mutants. (**C**) Quantification of bouton number at terminal branch of MNs for *D42*-driven white and *D42*-driven *unc-76* RNAi larvae, as indicated ($n = 30$ per genotype, 5 neurons per larva). Statistical analyses were performed with student's *t* test ($^{*}P < 0.05$, $^{**}P < 0.01$). (**D**) Cumulative survival trajectories of *D42*-driven white control flies and *D42*-driven *unc-76* RNAi flies. Statistical analysis was done using log-rank test ($^{*}P < 0.05$). (**E** and **F**) Climbing score of *D42*-driven white and *D42*-driven *unc-76* RNAi flies at (E) day 25 and (F) day 50 ($n = 5$, 25–30 flies for each set). Statistical analyses were performed with student's *t* test ($^{*}P < 0.05$, $^{**}P < 0.01$).

NMJ-associated synaptic boutons in drug treated but not in untreated mutant flies (Fig. 6D and E). Taken together, our results demonstrated that synaptic and locomotion deficits induced by UNC-76 deficiency may be ameliorated by pharmacological treatment with upstream activators of ATG1/UNC-51.

Discussion

A significant amount of knowledge about the transcriptional regulatory networks underlying the generation and specification of MNs is available. However, less is known about how the products from the genes expressed contribute to the development and function of MNs. Here, we show that FEZ1, whose encoding gene is deleted in JS patients, is highly expressed in the mammalian spinal cord. Using human ESC-derived MNs, we document that the onset of FEZ1 expression accompanies the commitment of neuroprogenitors to the MN lineage and continues to progressively rise over the course of development in hESC-derived MNs. Abrogation of FEZ1 expression strongly delays neurite elongation and maturation in developing MNs, with concomitant defects in transport of synaptic cargoes. Strikingly, MN-specific reduction of UNC-76 expression in *Drosophila* significantly reduced the number of synaptic boutons in NMJs

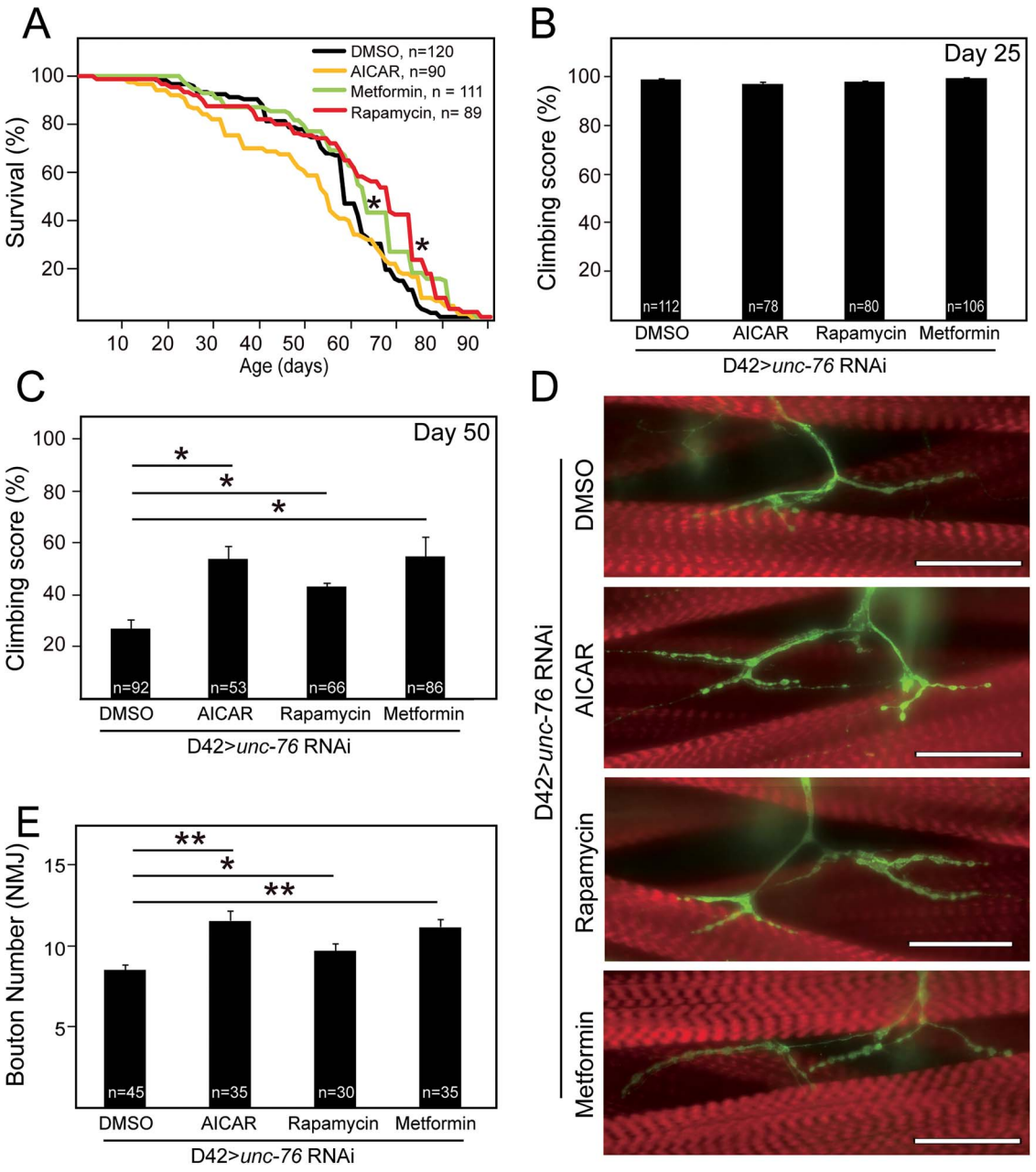

Figure 6. Pharmacological activation of ATG1 rescues pathological phenotypes in UNC-76-deficient *Drosophila*. (**A**) Cumulative survival trajectories of *D42 GAL4*-driven *unc-76* RNAi flies treated with drugs, as indicated ($n \geq 3$, 30 flies per set). Drug treatment was initiated on day 35 post-eclosion. Doses of AICAR, metformin and rapamycin used were at 0.1 mM, 1 mM and 200 µM, respectively. Statistical analysis was done using log-rank test ($^*P < 0.05$). (**B** and **C**) Climbing scores of drug-treated *D42 GAL4*-driven *unc-76* RNAi flies at day 25 and day 50, respectively ($n \geq 3$, 30 flies per set). DMSO was used as vehicle control for AICAR and rapamycin. *P*-values were determined by one-way ANOVA followed by Bonferroni's *post-hoc* test for specific comparisons of interest ($^*P < 0.05$). (**D**) Representative images of *D42*-driven *unc-76* RNAi larval NMJ double-stained with anti-HRP (green) to label MNs and phalloidin (red) for larval muscles. (**E**) Concentrations of AICAR, Rapamycin and Metformin used were 0.1 mM, 1 µM and 1 mM, respectively. Scale bar represents 50 µm. (**F**) Quantification of synaptic boutons at the axon termini of MNs ($n \geq 30$ MNs, 5 neurons per larva). Statistical analyses were performed with one-way ANOVA followed by Bonferroni's *post-hoc* test ($^*P < 0.05$, $^{**}P < 0.01$).

and is accompanied by locomotion deficits and early mortality. Remarkably, these deficits could be rescued by treatment with pharmacological compounds (including rapamycin, metformin and AICAR) that act on the FEZ1-activating kinase ATG1/UNC-51. Collectively, our results highlight a critical role of FEZ1 in MN development and the establishment of neuromuscular connections involved in locomotion behavior. Importantly, the phenotypes observed in *unc-76* mutant flies closely model motor impairments observed in JS patients.

Previous studies in nematode and fly models linked the loss of UNC-76 with locomotion defects (11,12,14). Subsequent studies on UNC-76 function unraveled its importance in the transport of synaptic proteins and the establishment of synapses via its role as a Kinesin-1 adapter (11–13). Using human MNs derived from ESCs, we confirm that FEZ1 is required for proper development of these neurons and that the observed retardation in development is associated with impaired cargo transport in the absence of FEZ1. Interestingly, complete abolishment of the

transport does not occur as synaptic cargoes emerged in neurites at an albeit a much later time point in comparison with control neurons. Intriguingly, while Piccolo can be observed to enter axons at DIV9, syntabulin, another Kinesin-1 adapter for active zone protein transport, is only weakly detected at DIV21 even though its levels peak in the spinal cord of newborn mice (35). This finding raises the possibility that a hitherto unidentified motor complex is involved in presynaptic cargo transport in the absence of FEZ1 at this stage of development.

While the direct impact on synapses has been shown in *unc-76* mutant worms, such effects have not been studied in genomic deletion of *Unc-76* in *Drosophila* (10). Our present results concur with previous studies and show that synaptic boutons are significantly reduced in NMJs formed by MNs of *unc-76* mutants. Importantly, we show that these abnormalities correlated directly with locomotion impairments in these mutants, thus demonstrating that loss of UNC-76 expression in MNs alone is sufficient to cause overt disruption of movement. Moreover, progressive mortality observed in *Drosophila* harboring *unc-76* germline mutations were recapitulated in both larval and adult mutant flies where UNC-76 ablation was restricted to MNs (12). Interestingly, although loss of FEZ1 function has been linked to abnormalities in dopaminergic transmission in FEZ1 knockout mice, we did not observe significant locomotor abnormalities in *Ddc-GAL4* driven *unc-76* RNAi flies even though declining survival rates also observed in these animals (36).

Motor impairment has been reported in most patients diagnosed with JS, a rare chromosomal disorder where large regions of the long arm of chromosome 11, frequently including the *FEZ1* locus, are deleted (15–17). While the clinical symptoms and regions of chromosomal deletion have been extensively characterized, significantly less is known about the underlying mechanisms involved. Of the deleted genes that have been studied, KIRREL3/Neph2 and ARHGAP32/PX-RICS have been linked to motor coordination. However, KIRREL3 knockout mice showed surprisingly similar, if not better, performance on rotarod tests as compared with control mice, which is contradictory to the symptoms in JS patients (37). In comparison, ARHGAP32-deficient mice performed poorly as compared with wild-type controls on the rotarod (38). These deficits were attributed to reduce surface expression of $GABA_A$ receptors in CNS neurons. Aside from these genes, *FEZ1* deletion is also frequently found in JS patients but its consequences towards development of the clinical symptoms in these patients are unknown (17,18). Our findings that loss of FEZ1 directly affects movement by impairing MN development and neuromuscular junction formation uncovers a hitherto important unknown mechanism involving the peripheral nervous system that can additionally contribute to delays in acquisition of gross and fine motor skills by JS patients.

FEZ1's function in axonal transport is positively regulated by phosphorylation of the evolutionarily conserved Serine 143 residue by ATG1 and MARK kinases and mutation in either kinase is sufficient to cause transport and synaptic defects (10,11). As specific pharmacological modulators of MARK kinases are unavailable, we decided to investigate if enhancing FEZ1 function by increasing ATG1 activity could ameliorate the phenotypic deficits observed in the *unc-76* RNAi mutant line. Strikingly, both synaptic and locomotion defects were ameliorated upon increasing ATG1 activity via its upstream pharmacological activators (rapamycin, AICAR and metformin) (Fig. 6). However, it is worth noting that the pharmacological modulators used are acting on upstream activators of ATG1; specifically, through master regulators AMPK and mTOR (33,39). As these kinases are involved in several downstream pathways besides the ATG1-UNC-76 pathway, we cannot exclude the possibility of these pathways contributing to the amelioration of defects observed in the *unc-76* RNAi mutant line. Multiple *Drosophila* and mouse studies have shown the possible involvement of S6K and PGC1α pathways in the rescue of locomotor deficits in various disease models (40–42). These two pathways are well documented to be downstream of mTOR and/or AMPK (43–46), and the alteration of these pathways could possibly contribute to the enhancement in locomotor activity in the flies. While we cannot completely eliminate the contribution of compensatory pathways triggered by the pharmacological intervention, these results suggest that the possible enhancement of ATG1 can help to rescue synaptic and locomotion defects when UNC-76 activity is compromised. Notably, rapamycin and metformin are already being prescribed for human use (47,48). Importantly, residual UNC-76 present in our *Drosophila* mutants mimics heterozygous loss of *FEZ1* in affected JS patients. Thus, it will be important in future studies to determine if activation of residual FEZ1 pool in these patients via administration of these drugs will also alleviate motor symptoms in JS patients.

Materials and Methods

Animals

Four male adult rats (Wistar) of 3 weeks of age were anesthetized with a cocktail comprising of ketamine (75 mg/kg) and xylazine (10 mg/kg) in 0.9% sodium chloride solution. Distinct parts of the brain such as temporal lobe, brain stem, prefrontal cortex, olfactory bulb, cerebellum, thalamus, striatum and hippocampus were dissected. The spinal cords were also harvested. All tissues were stored at −80°C till further use for immunoblot analyses.

IHC staining of spinal cord tissues

Four adult Wistar rats were used for this portion of the study. They were deeply anesthetized and perfused through the left cardiac ventricle with a solution of 4% paraformaldehyde and 0.1% glutaraldehyde in 0.1 M phosphate buffer (pH 7.4). The spinal cord was removed and sectioned transversely at 100 µm using a vibrating microtome (Leica, Wetzlar, Germany). The free-floating sections were washed with repeated changes of phosphate-buffered saline (PBS) for 3 h, and incubated overnight with a rabbit polyclonal antibody to FEZ1, diluted 1:500 in PBS. Sections were then incubated for 1 h in a 1:200 dilution of biotinylated anti-rabbit IgG (Vector, Burlingame, CA). This was followed by incubation with avidin–biotin complex for 1 h, and reaction with a mixture of 3,3′-diaminobenzidine tetrahydrochloride (Sigma-Aldrich, MO, USA) in nickel-Tris buffered saline containing 0.05% hydrogen peroxide for 5 min. The sections were counterstained with methyl green and coverslipped.

ChAT motor neurons differentiation

H1 hESC cell lines were kindly provided by Dr Soh Boon Seng. The hESCs were routinely passaged and maintained in mTESR™ 1 as described in the standard protocol (http://www.wicell.org). In order to generate $ChAT^+$ MNs, hESCs were dissociated with TrypLE™ Express (1x) and seeded on Matrigel-coated plates or coverslips at a ratio of 1:8. Media was replaced with a neural differentiation medium that comprised of DMEM/F12 and

Neurobasal medium at a 1:1 ratio supplemented with N2 (0.5x), B27 (0.5x), 0.1 mM ascorbic acid (Sigma-Aldrich), Glutamax (1x) and penicillin–streptomycin solution (1x). All media and cell dissociation components were purchased from Invitrogen. Small molecules including CHIR99021 (3 μM, Torcris), DMH1 (2 μM, Torcris) and SB431542 (2 μM, Torcris) were added into the medium and changed every 2 days for 8 days to induce NEP formation. NEP cells were dissociated again with TrypLE™ Express (1x) and seeded at 1:8 ratios with neural differentiation media containing 1 μM CHIR99021, 2 μM DMH1, 2 μM SB431542, 0.1 μM retinoic acid (RA, Torcris) and 0.5 μM purmorphamine (Pur, Torcris). Media was replaced every 2 days for 6 days to generate OLIG2$^+$ MNP P0. OLIG2$^+$ MNP P0 was passaged with TrypLE™ Express (1x) at 1:8 ratios with the same media for 7 days to generate OLIG2$^+$ MNP P1 and OLIG2$^+$ MNP P2. To induce MN formation, OLIG2$^+$ MNP cells were dissociated with TrypLE™ Express (1x) and plated at a 1:8 ratio on Matrigel-coated plates or coverslips with 0.5 μM RA, 0.1 μM Pur and 0.1 μM Compound E (Torcris) for 21 days. During all seeding procedures, ROCK inhibitor (Y-27632, STEMCELL Technologies) was added into the media to allow for adherence and survival of cells. At various time points, ChAT$^+$ MNs s were subjected to downstream IF assays or immunoblot analyses.

Generation of FEZ1 knockout ChAT motor neurons by CRISPR/Cas9 system

gRNA sequences targeting human FEZ1 gene (5′ AATCAGCTTC-AAGTCCATGG 3′) were designed using the online CRISPR design tool (http://crispr.mit.edu/) and inserted into LentiCRISPRv2 plasmid (Addgene, plasmid #52961) at the BsmBI restriction enzyme site. The Luc gRNA sequence was used as control (5′ CCGGGCTTTAACGAATATGA 3′). Resultant pLenti-CRISPR-FEZ1-KO vectors were co-transfected with pMDLg/pRRE, pRSV-rev and pMD2.G helper plasmids in a 2:1:1 ratio into HEK293 (13 000 000 cells/15 cm dish) in DMEM supplemented with 3% fetal bovine serum (FBS) for lentiviral production as described previously (49). At 4 to 6 h post transfection, medium was changed to DMEM/F12 medium (Sigma-Aldrich). Culture supernatants containing viruses were harvested 24 h post media change and passed through 0.45 μm filters. Concentration of lentiviruses were performed by ultracentrifugation at 3220 *g* for 30 min at 4°C via Amicon Ultra-15 filters (Millipore), after which they were snap-frozen in liquid nitrogen and stored in 100 μl aliquots at −80°C until use. To obtain FEZ1-knockout neurons, DIV1 MNs were infected with concentrated lentiviruses produced from pLenti-CRISPR-FEZ1-KO construct and were tested for FEZ1 expression through immunoassays at DIV7, DIV14 and DIV21 in MN culture media. Control MNs were infected with concentrated lentiviruses generated from pLenti-CRISPR-Luc construct that contained sgRNA targeting luciferase.

Immunoblotting experiments

For animal tissues, proteins were extracted using T-PER® Tissue Protein Extraction solution consisting of Halt protease inhibitor and 0.5 M EDTA (100x) (Invitrogen). hESC, NEP, OLIG2$^+$ MNP P0, OLIG2$^+$ MNP P2 and MNs were lysed with HEPES Lysis Buffer (50 mM HEPES, 150 mM NaCl, 1 mM EDTA, 1% Triton-X100, pH 7.2) supplemented with protease inhibitor cocktail (100x; Thermo Fisher Scientific). Lysates were clarified by centrifugation at 10 000 *g* for 10 min at 4°C. NuPAGE LDS Sample Buffer (4x, Thermo Fisher Scientific) was then added into lysates and stored at −20°C till further use. Quantifications of cell and animal tissue lysates were carried out using Pierce Protein Assay reagent (Thermo Fisher Scientific) at a wavelength of 660 nm. Prior to loading polyacrylamide gels, 15 μg of respective protein samples were denatured at 70°C for 10 min and loaded with designated protein ladder (Bio Basic) to be resolved by sodium dodecyl sulfate-polyacrylamide gel electrophoresis (SDS-PAGE). Resolved proteins were transferred to nitrocellulose membranes (Bio-Rad) using the Trans-Blot Turbo Transfer System (Bio-Rad) and blocked for 30 min with 5% non-fat milk (FairPrice) in TBST (150 mM Tris–HCl, pH 7.4, 1.5 M NaCl, 0.5% Tween20). Incubation of membranes with primary antibodies in 5% non-fat milk was carried out overnight at 4°C. After three washes with TBST washes for 5 min each, membranes were incubated with secondary antibodies in blocking reagent for an hour at 25°C. Before viewing respective protein bands in C-DiGit Chemiluminescence Western Blot Scanner (LI-COR), membranes were washed thrice with TBST for 5 min each and exposed to an enhanced chemiluminescent substrate (Thermo Fisher Scientific) for 5 min. Reprobing of membranes was performed after bound antibodies were detached with stripping buffer (15 g/L glycine, 1 g/L SDS, 1% Tween20, pH 2.2). Densitometric quantification was performed using ImageJ freeware and the relative band intensity was normalized to actin.

Primary antibodies utilized for immunoblotting experiments include: rabbit FEZ1 (1:1000, in-house), mouse synapsin-1 (1:1000, Millipore, MABN894), mouse SMI32 (1:4000, Millipore, NE1023), mouse OLIG2 (1:1000. Millipore, MABN50), rabbit ISL1 (1:1000, Abcam, ab109517), rabbit syntabulin (1:500, Proteintech, 16 972-1-AP), rabbit syntabulin (1:500, ThermoFisher Scientific, PA5-78529) and mouse β-actin (1:1000, Millipore, MAB1501). Secondary goat antibodies include horseradish peroxidase (HRP)-conjugated anti-mouse or rabbit IgG (H + L) antibody.

Immunofluorescence assays

After cells were fixed with 4% paraformaldehyde (PFA), coverslips were washed twice with PBS and exposed to 0.3% Triton-X100 (Sigma-Aldrich) in water for 10 min. After washing twice with PBS again, coverslips were blocked in 10% normal goat serum (NGS; Millipore) for 30 min and exposed to primary antibodies in blocking reagent at 25°C for an hour. Following three PBS washes for 10 min each, coverslips were incubated with secondary antibodies at 25°C for an hour. Coverslips were washed in PBS thrice and mounted with Fluoro-Gel II with DAPI (Electron Microscopy Sciences) on glass slides and visualized.

Primary antibodies used for IF include: rabbit Nanog (1:1000, Cell Signalling Technology, 3580S), rabbit Lin28a (1;2000, Cell Signalling Technology, 5930S), mouse Nestin (1:1000, Millipore, MAB5326), rabbit SOX2 (1:400, Synaptic Systems, 347 003), guinea pig βIII-tubulin (1:500, Synaptic Systems, 302 304), sheep HB9 (1:400, Abcam, ab59795), rabbit ISL1 (1:400, Abcam, ab109517), mouse OLIG2 (1:400. Millipore, MABN50), rabbit FEZ1 (1:400, in-house), mouse MAP2 (1:1000, Sigma-Aldrich, M9942), guinea-pig Tau (1:400, Synaptic Systems, 314 004), rabbit ChAT (1:1000, AB143, Millipore), mouse SMI32 (1:1000, Millipore, NE1023) and guinea pig Piccolo (1:400, 142 104, Synaptic Systems). Secondary donkey antibodies against mouse, guinea pig and rabbit were conjugated to either Cy2 or Cy3 or Cy5 dye (1:400, Jackson ImmunoResearch).

Fluorescence microscopy and image analyses

Images were acquired using a Zeiss Axio Observer Z1 Microscope equipped with a motorized stage. Total axon and dendrite

lengths were measured using semiautomatic tracing function via utilizing NeuronJ plugin of ImageJ. Complexity of dendrites and axons were examined by measuring the values of crossings at different distances using Sholl analysis plugin of Image J. Threshold was set to the circumference of the largest cell body/-clump before length or complexity analyses. MNs with proximal Piccolo puncta along neurites were manually counted and converted to cumulative percentages. Threshold for proximity was set at 50 µm.

Drosophila stocks and transgenic flies

Flies were maintained on standard yeast and cornmeal food at an average temperature of 25°C (50). Approximately 30 flies were collected per vial and the flies were transferred to vials containing fresh food every 2 days. Transgenic flies containing *D42-GAL4* (MN-specific driver), *Ddc*-GAL4 (dopaminergic neuron-specific driver), *Elav-GAL4* (pan-neuronal driver) and P{lacW}*unc-76*[G0310]/FM7c were all purchased from Bloomington *Drosophila* Stock Centre, USA. UAS-*unc-76* RNAi/TM3sb were purchased from Vienna Drosophila Resource Center, Austria. Heterozygous G0310 were created by crossing G0310/FM7i, P{Act GFP}TMR3 (balancer chromosome changed from FM7c) with w^{1118} flies. Knockdown of *unc-76* in specific neuronal types were generated by crossing with *Elav-GAL4* driver, *D42-GAL4* driver or *Ddc-GAL4* driver where the knockdowns were driven in a pan-neuronal fashion, in MNs specifically, or in dopaminergic neurons, respectively. Survival and locomotion assays were then conducted on the selected progeny.

RNA isolation and RT-PCR from adult flies

A total of 20 larval brains or 10 adult heads were collected and placed in 1.5 mL microcentrifuge tubes (Axygen, USA). Total RNA was harvested from these tissues by addition of TRIzol (Invitrogen, USA) and the tissues were homogenized with a plastic homogenizer before the addition of chloroform. Samples were centrifuged at 12 000 *g* for 15 min at 4°C and total RNA was collected from the aqueous phase after phase separation. RNA was left to precipitate overnight at −30°C after the addition of isopropanol. The mixture was centrifuged at 12 000 *g* for 10 min at 4°C and the resultant supernatant was carefully removed. The RNA pellet was then washed with 75% ethanol. Samples were then centrifuged at 7500 *g* for 5 min at 4°C and the washing step repeated once more. RNA pellets were then briefly air-dried and then reconstituted in diethylpyrocarbonate (DEPC)-treated water. The concentration of RNA was determined using a Nanodrop 2000 spectrophotometer (Thermoscientific, USA). To obtain cDNA, 500 ng of total RNA was reversed transcribed with SuperScript™ II Reverse Transcriptase (Invitrogen, USA) in 1x RT buffer containing 25 mM $MgCl_2$, 0.1 M DTT, 10 mM dNTP and 0.5 µg/µl oligo(dT). Polymerase chain reaction (PCR) of the cDNA was performed in 1x ThermoPol buffer (New England Biolabs Inc., USA) containing 10 mM dNTPs using gene specific primers. The *unc-76* forward primer (5′ TCGCTTATTGAAATCGGCCT 3′) and *unc-76* reverse primer (5′ ATGTCCAAATCGTTGGCCAC 3′) were used for PCR. Following which, 25 µl of the final PCR product were electrophoresed in a 1% (w/v) agarose gel in TAE buffer with SYBR® Safe DNA Gel Stain (Invitrogen, USA). After the run, the DNA bands were visualized under trans-UV light using Gel Doc™ XR+ Gel Documentation System (Bio-Rad, USA).

Preparation of lysates and immunoblot analysis

For the collection of protein lysates, either 20 larval brain or 12 adult heads were isolated and mixed with the radioimmunoprecipitation assay (RIPA) buffer (1% (v/v) Triton-X-100, 150 mM NaCl, 0.1% (w/v) SDS, 5 mM EDTA and 50 mM Tris–HCl, pH 7.5). Next, 10 µg/µl aprotonin and 1 mM PMSF were added into the mixture to inhibit protease activities. Homogenization was carried out with a plastic homogenizer before samples were centrifuged at 15 000 *g* for 10 min at 4°C. The supernatant was collected and placed in a new microcentrifuge tube (Axygen, USA). The lysates for immunoblot were diluted in 2x SDS loading buffer, boiled at 100°C for 5 min before being loaded on 10% SDS-PAGE. Precision Plus Protein™ Unstained Standards (Bio-rad, USA) were used as protein ladders in protein gel. Protein was transferred onto a nitrocellulose membrane (Whatman, Germany) using the wet transfer technique with 10% methanol transfer buffer. After the transfer, the membrane was blocked with blocking buffer containing 5% non-fat milk in TBST (25 mM Tris–HCl, pH 7.4, 137 mM NaCl, 2.68 mM KCl, and 0.05% Tween 20) for 1 h at room temperature. The membranes were subsequently incubated with antibodies against FEZ1 (antibody 361) or β-tubulin (clone E7) (Developmental Studies Hybrodima Bank, USA) overnight at 4°C. The next day, the membranes were washed three times with TBST for 10 min each. HRP-conjugated secondary antibodies against either rabbit or mouse antibodies diluted in TBST were then added and incubated for 1 h at room temperature. Membranes were then washed thrice with TBST for 10 min each. Bands were visualized by exposing the membrane to Pierce ECL Western Blotting Substrate (Pierce, USA) or WesternBright Sirius Western Blotting detection kit (Advansta, USA) using the Classic Blue film (MIDSCI, USA). Film was developed using Medical X-ray Processor 2000 (Carestream Health, USA).

Immunohistochemistry of larval neuromuscular junction

Day 4 larvae (late second instar) were dissected in PBS and fixed in 5% (v/v) formaldehyde in PBS for an hour before blocking in 5% (v/v) NGS in PBS for another hour. The larval body walls were then incubated in primary antibody overnight. The next day, sections were washed three times before incubation with fluorescent conjugated secondary antibodies for 2 h, which was followed by another round of washing. Samples were then mounted in VectaShield (Vector Laboratories) for microscopic analysis. Primary antibodies against Fasciclin (Developmental Hybridoma Studies Bank, USA) and Futsch (Developmental Hybridoma Studies Bank, USA) were used to stain MNs at a dilution of 1:20. Following the primary incubation, Alexa-488-conjugated α-mouse (Molecular Probes, USA) and Atto 647 N conjugated phalloidin (Sigma-Aldrich, USA) were used as secondary antibody. Quantification of synaptic boutons was performed at the terminal branch of NMJ, where a bouton is defined as a terminal swelling of a branch.

Imaging and microscopy

Visualization of immunohistochemistry samples were performed through the IX83 Inverted Microscope (Olympus, USA) with 20x magnification and accompanying software, cellSens. Images were processed in ImageJ (National Institutes of Health, USA) and Adobe Photoshop software (Adobe Systems, USA). Selection of larvae based on the presence of GFP was also

conducted through visualization under the IX83 Inverted Microscope (Olympus, USA) at 10x magnification.

Larval crawling assay

Day 4 larvae (late second instar) were collected and individually placed on the designated starting point in the middle of the 60 mm SYLGARD® silicone dish (DOWSIL™, USA). The trailing paths that the larvae traveled within 2 min on the dish was traced on the lid of the dish and measured. Sixty larvae were collected for each genotype. The average body length per min (instead of average distance) was calculated to account for the differences in body length that could affect the crawling distance of each individual larva. Larvae that were not crawling were disregarded from the assay. Each data point represents the data collected from one single larva.

Adult flies survival assay

Flies were maintained on standard yeast and cornmeal food at an average temperature of 25°C. Approximately 5 pairs of flies (5 females) were allowed to lay eggs for 24 h so as to obtain synchronously developing cohorts of flies for experiments. For each experimental group, 89–120 female flies were collected, with approximately 30 adult flies per vial, and the mortality was monitored on alternating days.

Fly climbing assay

The climbing assays were all arranged to be conducted 1 day after changing of food. Between 20 and 30 female flies were collected for each vial. Flies were anaesthetized by CO_2 and placed into a cylindrical column (30 cm in length and 1.5 cm in diameter), and were left to recovered at 25°C for 2 h. Flies were gently tapped to the bottom of the column and the number of flies that crossed the 11 cm mark on the cylindrical rod within the time limit of 20 s was recorded. The same set of flies were repeated for 6 trials in total with intervals of 1 min, and the average of the 6 technical replicates was plotted as a single point. Each data point represents 20–30 flies.

Pharmacological modulation

To study the effect of drugs, different drugs were mixed into the cornmeal food in their respective concentrations and given to flies starting from day 35. About 0.1 mM AICAR (Cayman Chemicals), 200 μM rapamycin and 1 mM metformin were supplemented into the food. Drug-infused food was given to the flies for a period of 15 days till day 50, when the climbing scores were recorded.

Statistical analysis

Quantitative values are means ± S.E.M. or ± SD. Statistical significance was determined using Unpaired Student's *t*-test or one-way ANOVA, followed by Bonferroni's *post-hoc* test for specific comparisons of interest. $^{*}P < 0.05$, $^{**}P < 0.01$, $^{***}P < 0.001$, $^{***}P < 0.0001$. The log-rank test was used to estimate the statistical difference between the survival curves of the samples ($^{*}P < 0.05$).

Supplementary Material

Supplementary Material is available at *HMG* online.

Acknowledgements

The authors are grateful to Brian Kennedy for critical comments. Technical help from Ms Rachel Woon-Sim Koh for immunohistochemistry is acknowledged.

Conflict of Interest statement: The authors declare no competing financial interests.

Funding

National Medical Research Council Large Collaborative Grant in Parkinson's disease (SPARK2), and the Singapore Ministry of Education (T1-2015 April-03) and funding from Institute for Health Innovation and Technology (JJEC).

References

1. Pfenninger, K.H. (2009) Plasma membrane expansion: a neuron's Herculean task. *Nat. Rev. Neurosci.*, **10**, 251–261.
2. Nirschl, J.J., Ghiretti, A.E. and Holzbaur, E.L.F. (2017) The impact of cytoskeletal organization on the local regulation of neuronal transport. *Nat. Rev. Neurosci.*, **18**, 585–597.
3. Franker, M.A. and Hoogenraad, C.C. (2013) Microtubule-based transport - basic mechanisms, traffic rules and role in neurological pathogenesis. *J. Cell Sci.*, **126**, 2319–2329.
4. Hirokawa, N., Niwa, S. and Tanaka, Y. (2010) Molecular motors in neurons: transport mechanisms and roles in brain function, development, and disease. *Neuron*, **68**, 610–638.
5. Millecamps, S. and Julien, J.P. (2013) Axonal transport deficits and neurodegenerative diseases. *Nat. Rev. Neurosci.*, **14**, 161–176.
6. Fu, M.M. and Holzbaur, E.L. (2014) Integrated regulation of motor-driven organelle transport by scaffolding proteins. *Trends Cell Biol.*, **24**, 564–574.
7. Stowers, R.S., Megeath, L.J., Gorska-Andrzejak, J., Meinertzhagen, I.A. and Schwarz, T.L. (2002) Axonal transport of mitochondria to synapses depends on Milton, a novel Drosophila protein. *Neuron*, **36**, 1063–1077.
8. Glater, E.E., Megeath, L.J., Stowers, R.S. and Schwarz, T.L. (2006) Axonal transport of mitochondria requires Milton to recruit kinesin heavy chain and is light chain independent. *J. Cell Biol.*, **173**, 545–557.
9. Cai, Q., Gerwin, C. and Sheng, Z.H. (2005) Syntabulin-mediated anterograde transport of mitochondria along neuronal processes. *J. Cell Biol.*, **170**, 959–969.
10. Butkevich, E., Hartig, W., Nikolov, M., Erck, C., Grosche, J., Urlaub, H., Schmidt, C.F., Klopfenstein, D.R. and Chua, J.J. (2016) Phosphorylation of FEZ1 by microtubule affinity regulating kinases regulates its function in presynaptic protein trafficking. *Sci. Rep.*, **6**, 26965.
11. Toda, H., Mochizuki, H., Flores, R., 3rd, Josowitz, R., Krasieva, T.B., Lamorte, V.J., Suzuki, E., Gindhart, J.G., Furukubo-Tokunaga, K. and Tomoda, T. (2008) UNC-51/ATG1 kinase regulates axonal transport by mediating motor-cargo assembly. *Genes Dev.*, **22**, 3292–3307.
12. Gindhart, J.G., Chen, J., Faulkner, M., Gandhi, R., Doerner, K., Wisniewski, T. and Nandlestadt, A. (2003) The kinesin-associated protein UNC-76 is required for axonal transport in the Drosophila nervous system. *Mol. Biol. Cell*, **14**, 3356–3365.

13. Chua, J.J., Butkevich, E., Worseck, J.M., Kittelmann, M., Gronborg, M., Behrmann, E., Stelzl, U., Pavlos, N.J., Lalowski, M.M., Eimer, S. *et al*. (2012) Phosphorylation-regulated axonal dependent transport of syntaxin 1 is mediated by a Kinesin-1 adapter. *Proc. Natl. Acad. Sci. U. S. A.*, **109**, 5862–5867.
14. Bloom, L. and Horvitz, H.R. (1997) The *Caenorhabditis elegans* gene unc-76 and its human homologs define a new gene family involved in axonal outgrowth and fasciculation. *Proc. Natl. Acad. Sci. U. S. A.*, **94**, 3414–3419.
15. Favier, R., Akshoomoff, N., Mattson, S. and Grossfeld, P. (2015) Jacobsen syndrome: advances in our knowledge of phenotype and genotype. *Am. J. Med. Genet. C Semin. Med. Genet.*, **169**, 239–250.
16. Mattina, T., Perrotta, C.S. and Grossfeld, P. (2009) Jacobsen syndrome. *Orphanet J. Rare Dis.*, **4**, 9.
17. Grossfeld, P.D., Mattina, T., Lai, Z., Favier, R., Jones, K.L., Cotter, F. and Jones, C. (2004) The 11q terminal deletion disorder: a prospective study of 110 cases. *Am. J. Med. Genet. A*, **129A**, 51–61.
18. Penny, L.A., Dell'Aquila, M., Jones, M.C., Bergoffen, J., Cunniff, C., Fryns, J.P., Grace, E., Graham, J.M., Jr., Kousseff, B., Mattina, T. *et al*. (1995) Clinical and molecular characterization of patients with distal 11q deletions. *Am. J. Hum. Genet.*, **56**, 676–683.
19. Honda, A., Miyoshi, K., Baba, K., Taniguchi, M., Koyama, Y., Kuroda, S., Katayama, T. and Tohyama, M. (2004) Expression of fasciculation and elongation protein zeta-1 (FEZ1) in the developing rat brain. *Brain Res. Mol. Brain Res.*, **122**, 89–92.
20. Fujita, T., Ikuta, J., Hamada, J., Okajima, T., Tatematsu, K., Tanizawa, K. and Kuroda, S. (2004) Identification of a tissue-non-specific homologue of axonal fasciculation and elongation protein zeta-1. *Biochem. Biophys. Res. Commun.*, **313**, 738–744.
21. Arber, S. (2012) Motor circuits in action: specification, connectivity, and function. *Neuron*, **74**, 975–989.
22. Desai, C., Garriga, G., McIntire, S.L. and Horvitz, H.R. (1988) A genetic pathway for the development of the *Caenorhabditis elegans* HSN motor neurons. *Nature*, **336**, 638–646.
23. Du, Z.W., Chen, H., Liu, H., Lu, J., Qian, K., Huang, C.L., Zhong, X., Fan, F. and Zhang, S.C. (2015) Generation and expansion of highly pure motor neuron progenitors from human pluripotent stem cells. *Nat. Commun.*, **6**, 6626.
24. Park, S., Kim, J.Y., Myung, S., Jung, N., Choi, Y. and Jung, S.C. (2019) Differentiation of motor neuron-like cells from tonsil-derived mesenchymal stem cells and their possible application to neuromuscular junction formation. *Int. J. Mol. Sci.*, **20**, 2702.
25. Wilson, M.D., Sethi, S., Lein, P.J. and Keil, K.P. (2017) Valid statistical approaches for analyzing sholl data: mixed effects versus simple linear models. *J. Neurosci. Methods*, **279**, 33–43.
26. Adalbert, R., Nogradi, A., Babetto, E., Janeckova, L., Walker, S.A., Kerschensteiner, M., Misgeld, T. and Coleman, M.P. (2009) Severely dystrophic axons at amyloid plaques remain continuous and connected to viable cell bodies. *Brain*, **132**, 402–416.
27. Nishimune, H., Badawi, Y., Mori, S. and Shigemoto, K. (2016) Dual-color STED microscopy reveals a sandwich structure of Bassoon and Piccolo in active zones of adult and aged mice. *Sci. Rep.*, **6**, 27935.
28. Cai, Q., Pan, P.Y. and Sheng, Z.H. (2007) Syntabulin-kinesin-1 family member 5B-mediated axonal transport contributes to activity-dependent presynaptic assembly. *J. Neurosci.*, **27**, 7284–7296.
29. Kohsaka, H., Guertin, P.A. and Nose, A. (2017) Neural circuits underlying fly larval locomotion. *Curr. Pharm. Des.*, **23**, 1722–1733.
30. Jones, M.A. and Grotewiel, M. (2011) Drosophila as a model for age-related impairment in locomotor and other behaviors. *Exp. Gerontol.*, **46**, 320–325.
31. Ng, C.H., Mok, S.Z., Koh, C., Ouyang, X., Fivaz, M.L., Tan, E.K., Dawson, V.L., Dawson, T.M., Yu, F. and Lim, K.L. (2009) Parkin protects against LRRK2 G2019S mutant-induced dopaminergic neurodegeneration in Drosophila. *J. Neurosci.*, **29**, 11257–11262.
32. Egan, D.F., Shackelford, D.B., Mihaylova, M.M., Gelino, S., Kohnz, R.A., Mair, W., Vasquez, D.S., Joshi, A., Gwinn, D.M., Taylor, R. *et al*. (2011) Phosphorylation of ULK1 (hATG1) by AMP-activated protein kinase connects energy sensing to mitophagy. *Science*, **331**, 456–461.
33. Kim, J., Kundu, M., Viollet, B. and Guan, K.L. (2011) AMPK and mTOR regulate autophagy through direct phosphorylation of Ulk1. *Nat. Cell Biol.*, **13**, 132–141.
34. Lee, J.W., Park, S., Takahashi, Y. and Wang, H.G. (2010) The association of AMPK with ULK1 regulates autophagy. *PLoS One*, **5**, e15394.
35. Xiong, G.J., Cheng, X.T., Sun, T., Xie, Y., Huang, N., Li, S., Lin, M.Y. and Sheng, Z.H. (2020) Defects in syntabulin-mediated synaptic cargo transport associate with autism-like synaptic dysfunction and social behavioral traits. *Mol. Psychiatry*, in press.
36. Sakae, N., Yamasaki, N., Kitaichi, K., Fukuda, T., Yamada, M., Yoshikawa, H., Hiranita, T., Tatsumi, Y., Kira, J., Yamamoto, T. *et al*. (2008) Mice lacking the schizophrenia-associated protein FEZ1 manifest hyperactivity and enhanced responsiveness to psychostimulants. *Hum. Mol. Genet.*, **17**, 3191–3203.
37. Volker, L.A., Maar, B.A., Pulido Guevara, B.A., Bilkei-Gorzo, A., Zimmer, A., Bronneke, H., Dafinger, C., Bertsch, S., Wagener, J.R., Schweizer, H. *et al*. (2018) Neph2/Kirrel3 regulates sensory input, motor coordination, and home-cage activity in rodents. *Genes Brain Behav.*, **17**, e12516.
38. Nakamura, T., Arima-Yoshida, F., Sakaue, F., Nasu-Nishimura, Y., Takeda, Y., Matsuura, K., Akshoomoff, N., Mattson, S.N., Grossfeld, P.D., Manabe, T. *et al*. (2016) PX-RICS-deficient mice mimic autism spectrum disorder in Jacobsen syndrome through impaired GABAA receptor trafficking. *Nat. Commun.*, **7**, 10861.
39. Jung, C.H., Jun, C.B., Ro, S.H., Kim, Y.M., Otto, N.M., Cao, J., Kundu, M. and Kim, D.H. (2009) ULK-Atg13-FIP200 complexes mediate mTOR signaling to the autophagy machinery. *Mol. Biol. Cell*, **20**, 1992–2003.
40. Ng, C.H., Basil, A.H., Hang, L., Tan, R., Goh, K.L., O'Neill, S., Zhang, X., Yu, F. and Lim, K.L. (2017) Genetic or pharmacological activation of the Drosophila PGC-1alpha ortholog spargel rescues the disease phenotypes of genetic models of Parkinson's disease. *Neurobiol. Aging*, **55**, 33–37.
41. Zhao, W., Varghese, M., Yemul, S., Pan, Y., Cheng, A., Marano, P., Hassan, S., Vempati, P., Chen, F., Qian, X. *et al*. (2011) Peroxisome proliferator activator receptor gamma coactivator-1alpha (PGC-1alpha) improves motor performance and survival in a mouse model of amyotrophic lateral sclerosis. *Mol. Neurodegener.*, **6**, 51.
42. Kinghorn, K.J., Gronke, S., Castillo-Quan, J.I., Woodling, N.S., Li, L., Sirka, E., Gegg, M., Mills, K., Hardy, J., Bjedov, I. and Partridge, L. (2016) A Drosophila model of Neuronopathic Gaucher disease demonstrates lysosomal-autophagic defects and altered mTOR signalling and

is functionally rescued by rapamycin. *J. Neurosci.*, **36**, 11654–11670.
43. Canto, C. and Auwerx, J. (2009) PGC-1alpha, SIRT1 and AMPK, an energy sensing network that controls energy expenditure. *Curr. Opin. Lipidol.*, **20**, 98–105.
44. Cunningham, J.T., Rodgers, J.T., Arlow, D.H., Vazquez, F., Mootha, V.K. and Puigserver, P. (2007) mTOR controls mitochondrial oxidative function through a YY1-PGC-1alpha transcriptional complex. *Nature*, **450**, 736–740.
45. Fenton, T.R. and Gout, I.T. (2011) Functions and regulation of the 70kDa ribosomal S6 kinases. *Int. J. Biochem. Cell Biol.*, **43**, 47–59.
46. Wan, Z., Root-McCaig, J., Castellani, L., Kemp, B.E., Steinberg, G.R. and Wright, D.C. (2014) Evidence for the role of AMPK in regulating PGC-1 alpha expression and mitochondrial proteins in mouse epididymal adipose tissue. *Obesity (Silver Spring)*, **22**, 730–738.
47. Hostalek, U., Gwilt, M. and Hildemann, S. (2015) Therapeutic use of metformin in prediabetes and diabetes prevention. *Drugs*, **75**, 1071–1094.
48. Li, J., Kim, S.G. and Blenis, J. (2014) Rapamycin: one drug, many effects. *Cell Metab.*, **19**, 373–379.
49. Yagensky, O., Kohansal-Nodehi, M., Gunaseelan, S., Rabe, T., Zafar, S., Zerr, I., Hartig, W., Urlaub, H. and Chua, J.J. (2019) Increased expression of heme-binding protein 1 early in Alzheimer's disease is linked to neurotoxicity. *Elife*, **8**, e47498.
50. Dillon, M.E., Wang, G., Garrity, P.A. and Huey, R.B. (2009) Review: thermal preference in Drosophila. *J. Therm. Biol.*, **34**, 109–119.